Multi-carrier Visible Light Communication System Using Enhanced Sub-carrier Index Modulation and Discrete Wavelet Transform

Arslan Khalid[1] · Faizan Rashid[2] · Umair Tahir[2] · Hafiz M. Asif[3] · Fadi Al-Turjman[4]

Abstract

This work is aimed at providing a novel design of the Visible Light Communication (VLC) system that uses the Multi-Carrier Code-Division Multiple Access (MC-CDMA) technique to send and receive data through intensity-modulated/direct detected (IM/DD) VLC channel. The state-of-the-art framework of Enhanced Sub-Carrier Index Modulation (ESIM) is utilized to reduce the inherent peak-to-average power ratio (PAPR) in Orthogonal Frequency Division Multiplexing. Additionally, the use of cyclic prefix is omitted through the Discrete Wavelet Transform in the current system. Hence, the performance of the system is optimized in terms of PAPR, Bit Error Rate (BER), and data rate. The work presents the closed-form BER expressions for both conventional and proposed techniques in line-of-sight VLC channel. Correspondingly, the simulation programs are also executed to compared the proposed ESIM based WT-MC-CDMA system with both existing systems followed by an analysis of the results. Simulation results show the superior performance of the proposed system compared to existing systems.

Keywords BER · CCDF · DFT · DWT · LED · MC-CDMA · PAPR

✉ Arslan Khalid
engr.arslan08@gmail.com

1   School of Information, Computer, and Communication Technology, Sirindhorn International Institute of Technology, Bangkadi, Mueang, Pathum Thani 12000, Thailand

2   Department of Electrical Engineering, The University of Lahore, Defence Road, Lahore 54000, Pakistan

3   Department of Electrical and Computer Engineering, Sultan Qaboos University, Muscat, Oman

4   Artificial Intelligence Engineering Department, Research Center for AI and IoT, Near East University, Nicosia, Mersin 10, Turkey

1 Introduction

The continually growing demands of higher data-rates, device connectivity, and smaller latency have compelled telecom service providers to switch their wireless communication systems from fourth-generation 4G to the new one, commonly termed as fifth-generation 5G. The long-term goals and visions of 5G communication systems lie in offering a complete solution that enables both voice and high-speed data traffic to users at any point, anytime, and anywhere [1, 2]. Nonetheless, the scarcity of traditional radio frequency (RF) spectrum set limits in achieving these goals for wireless communications. With current technology modernizations in the computing era i.e., the Internet of Things (IoT) where every device is capable of providing connectivity and processing will necessitate more updated technology [3, 4]. In such circumstances, there is a dire need to emphasize on emerging wireless technologies; Visible Light Communication (VLC) is one of them that can mitigate the scarcity of RF spectra. The VLC system uses prevailing lighting infrastructure with the addition of a communication chip to understand the functionality of lighting and high-speed data communications concurrently. VLC transmitters are realized via LEDs or laser-diodes that can transfer the information by the fast flickering of light (on and off) while the receiver uses photo-diodes to detect the changing intensity of light [5–7].

In comparison with the RF-based wireless communication system, VLC provides interference-free bandwidth of approximately 300 THz, which is significantly broader than RF. Moreover, the process of license permission is not mandatory [8]. The other key merits include inherent secure communication as the light signals do not penetrate through non-transparent objects, high-quality service, and inexpensive optoelectronic components, harmless to human bodies, and no electromagnetic interference (EMI) [9]. From this perspective, it is commonly used in airplanes, hospitals, intelligent transportation systems, undersea communications, and indoor positioning, etc. that have been vulnerable to EMI or safety concerns [10, 11].

A VLC system uses pulse modulation schemes like on–off keying (OOK), pulse-position modulation (PPM), and pulse-amplitude modulation (PAM) as an obvious choice. However, as data-rates of VLC system approaches to hundreds of megabits per second or even more, these modulation techniques put limits on spectral and power efficiency due to inter-symbol interference (ISI) [12]. To overcome the aforesaid issues, the MC-CDMA technique draws the attention of various researchers, since it makes maximum use of available restricted bandwidth and takes good care of severe ISI that occurs mainly because of high data-rates [13–17]. MC-CDMA is a combination of a multi-carrier scheme called Orthogonal Frequency Division Multiplexing (OFDM) and CDMA. The central idea of utilizing OFDM transmission within a CDMA technique is to maximize the symbol period to ensure that a frequency selective fading channel is split up into several narrowband flat fading channels [17].

A typical MC-CDMA modem is developed by applying Inverse Discrete Fourier Transform (IDFT) block at the transmitter and Discrete Fourier Transform (DFT) block at the receiver respectively. With these blocks, sinusoidal waveforms are used as sub-carriers that are not well-localized in the time domain. Thereby, a cyclic prefix (CP) is positioned in between the successive OFDM symbols that will not only exclude the ISI but also provides a solution for Inter-Channel Interference (ICI) [17]. In practice, the length of the CP is 1/4th of the modulating waveform and it acts as an overhead that alleviates the data-rate, energy, and bandwidth efficiency. Further, another negative aspect of OFDM is high PAPR which also degrades the effectiveness of optical MC-CDMA transmission [18].

To address the aforementioned intrinsic issues of OFDM, numerous techniques are suggested in the literature that confines the PAPR and exterminates the utilization of CP in the traditional OFDM based communication system. In this connection, the work done in [19] expresses that a transmitted signal can be changed from stationary characteristics to cyclo-stationary with the help of an overlapped pulse shaping filter. The key concept of this technique is to attain time localization. Nevertheless, this technique needs to optimize filter parameters for pulse shaping which is a tedious task to do. While in [20], a blind channel estimation technique is engaged in OFDM design that eradicates the CP by exploiting the Toeplitz channel matrix. The benefit of this technique lies in the higher data-rate and bandwidth efficiency. Conversely, this technique increases the computational complexity of the receiver.

The subspace methods for the detection of the MC-CDMA signal without CP are employed in [21], however, the computational complexity is the main concern in such methods. A time-domain equalizer was offered in [22] that reduces the delay spread of the channel. Likewise, an MMSE algorithm was also proposed for channel shortening [23]. In [24], a block coding based multi-carrier scheme is proposed for the reduction of PAPR that parades higher performance but at lower bit rates. Later, clipping and filtering based multi-carrier technique [25] is also proposed that delivers acceptable results but at the outlay of quantifiable distortion. Meanwhile, Muller et. al [26] and Bauml et. al [27] have suggested probabilistic methods that curb the PAPR within an OFDM system. These reduction techniques portray efficient distortionless PAPR results, yet, these techniques face a serious disadvantage, i.e., the computational complexity of the system surges due to the rise in the number of DFT points. It is also pertinent to state here that all previously mentioned proposed techniques have a common demerit of maximizing the computational complexity of the receiver that is divergent to the basic design of MC-CDMA.

To generate the MC-CDMA symbol, the current work cascaded the enhanced form of OFDM, which is characterized as enhanced sub-carrier index-modulation OFDM (ESIM) with the CDMA scheme. Moreover, to improve the performance of the proposed system the traditional Fourier transforms are swap with the wavelet transforms (WT). The proposed system appears to be a good remedy for both CP and PAPR concerns of OFDM. ESIM with its state-of-the-art framework wrestles the problem of high PAPR while wavelet techniques carry excellent orthogonal properties due to which CP is no more necessary between the two consecutive symbols. Hence, the spectral efficiency of the system is amended to some extent. With WT, the system also turns out to be more robust to ISI as the side-lobes of the wavelet-based OFDM system are much lower when compared with the Fourier transform-based system. Therefore, the overall energy of the system is also conserved [28].

This work presents the comparative analysis for OFDM based MC-CDMA, ESIM based FT-MC-CDMA and ESIM based WT-MC-CDMA in the existence of a line-of-sight (LoS) environment. OFDM based MC-CDMA technique is used as a benchmark while the proposed techniques are compared with it. For the qualitative and quantitative performance assessment of any system, an analytical expression is used to obtain more accurate results. Therefore, exact closed-form mathematical expressions for BER of IM/DD optical systems based on the proposed techniques are also derived and provided in the work. The computer programs are developed in MATLAB tool while the main performance metrics for the aforementioned systems are BER and PAPR. The simulation results are produced exclusively to validate the derived analytical expressions.

Additionally, the work also offers a series of simulation results with a detailed description of the visible light characteristics.

The entire research article is planned in the succeeding sections. Section 2 contributes a comprehensive description of the systems modeling. This section also illustrates the mathematical equations to compute an impulsive response of the VLC channel. Later, in Sect. 3 the analytical BER expressions for the conventional and proposed systems are derived that will help in performance assessment. While Sect. 4 shows the simulation results with significant discussions. The last section will conclude the complete work.

2 Analytical System Modeling

This section presents a thorough discussion of the VLC system design for both Fourier and Wavelet-based MC-CDMA techniques. Further, a brief description of the VLC channel employed for the computer simulations is also delineated.
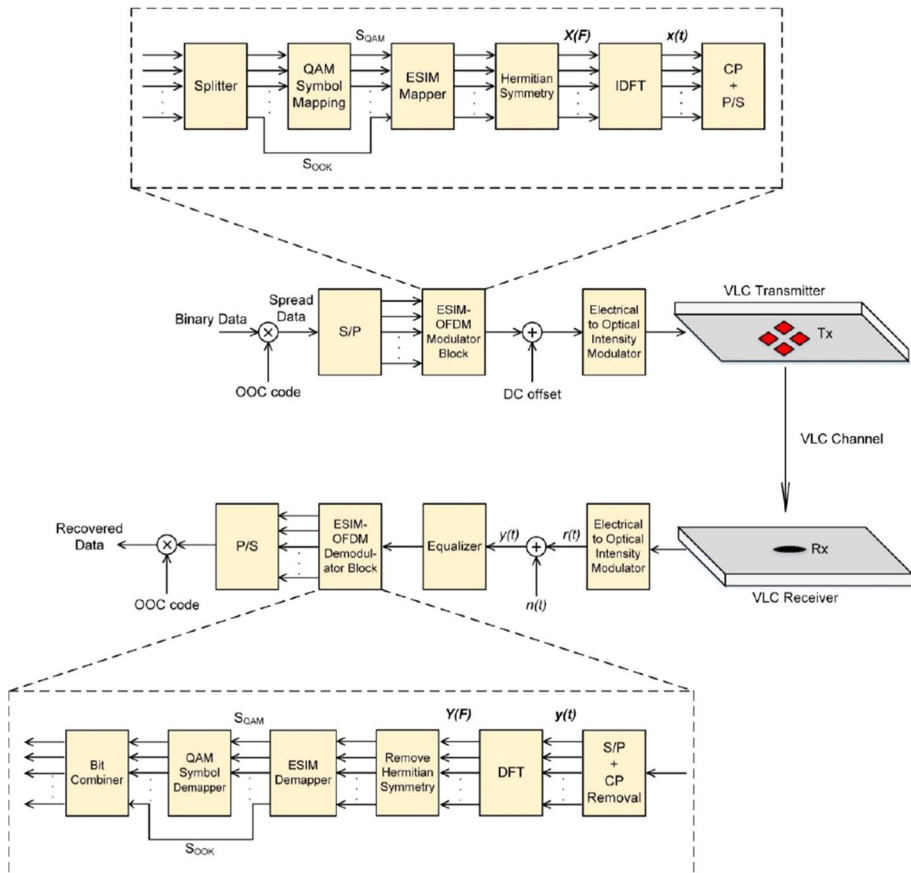

Fig. 1 VLC system design for DFT based MC-CDMA

2.1 Discrete Fourier Transform Based MC-CDMA Technique

The VLC system for ESIM based FT-MC-CDMA technique is demonstrated in Fig. 1. Binary data from the user are first multiplied by the Optical Orthogonal Code (OOC) code. OOC codes are the family of unipolar (0,1) codes that exhibit brilliant cross-correlation and autocorrelation properties. These codes are closely linked to constant weight error-correcting codes and therefore, they can also introduce link reliability in the proposed system. The code length of the OOC is selected to be 7 while the code weight is 3. After the spreading/encoding of binary data, the resultant sequence is divided into parallel sub-carriers and then input to the ESIM-OFDM modulator.

In the ESIM-OFDM modulator, initially, the sub-carriers are split into two subsequences namely S_{OOK} and S_{QAM}. Subsequence S_{OOK} is employed to represent the capacity of two sub-carriers (active and inactive) while S_{QAM} shows constellation points transmitted within the sub-carriers [29]. In the subsequent step, the mapper traverses the complete OOK subsequence and if the mapper found that the OOK bit is 1 then a pair of sub-carriers is selected. The first sub-carrier is an active one and it transmits the QAM symbol while the other sub-carrier is inactive. The inactive sub-carrier conveys no information and ideally, it is assumed that it has no energy. Moreover, if the OOK bit is found to be 0, then the first sub-carrier of the pair is inactive while the other has a QAM symbol. In this manner, the complete operation is done on every OOK bit of subsequence, and sub-carriers are formed.

To ensure a real-valued and non-negative modulating waveform necessary for the IM/DD, Hermitian symmetry is levied on the incoming signals before applying the IDFT operation [30]. The sub-carriers are then supplied to the IDFT block that shifts them from the frequency domain to the time domain and later CP or guard intervals are added between two consecutive ESIM symbols. After CP insertion, the data within the sub-carriers are serially combined and it is noticeable that the modulating waveform is still bipolar. Therefore, proper convergence into a unipolar signal is necessary and for this, DC offset is added in the MC-CDMA waveform. At this point, it is worth telling here that due to the inherent PAPR issue of MC-CDMA a higher DC offset is obligatory to completely exclude the negative peaks which in turn increases the optical energy-per-bit to single-sided noise power-spectral density, $E_{b_{(opt)}}/N_0$, hence, the optical energy is not conserved [31]. So, a suitable DC offset is added and the leftover negative peaks are clipped to zero. In the last step, the DFT based MC-CDMA waveform is provided to the ideal optical modulator wherein the optical intensity is produced with the input electrical signal. The optical signal is then moved through the free-space medium.

The photo-diode positioned at the receiver side gathers the optical signal which is degraded by the free-space VLC channel. After optical to electrical convergence, a shot noise which is modeled as additive white Gaussian noise (AWGN) is included in the electrical domain. The noise added electrical signal is applied to the sub-optimal zero forcing equalizer that diminishes the channel effects. Subsequently, the serial data is transformed back to the parallel sub-carriers and the CP is removed. Moreover, the time domain signals are also transmuted back to the frequency domain using DFT block and the signals are making free of Hermitian symmetry. The recovered signals are applied to the demapper that separates the two sequences S_{OOK} and S_{QAM}. This can be done by applying the comparator approach on a pair of consecutive sub-carriers. The magnitude of both sub-carriers is computed and compared with each other [32].

Let's consider a case in which the magnitude of the first sub-carrier is greater than the second sub-carrier. The comparator decides that the first sub-carrier is an active one and it contains a QAM symbol. While the corresponding OOK bit is detected as 1. In the meantime, the second sub-carrier of the pair is detected as an inactive. Similarly, if the magnitude of the first sub-carrier is less than the second, then, in that case, the comparator decides that the first sub-carrier is inactive while the second has a QAM symbol. The corresponding OOK bit with this sub-carrier is detected as zero. Likewise, all sub-carrier pairs are traversed by the demapper, and subsequences (S_{OOK} and S_{QAM}) are separated and then combined to form a single bitstream. This stream is then multiplied with the spreading waveform to get the original bitstream.

2.2 Discrete Wavelet Transform Based MC-CDMA Technique

The existing section enlightens the framework for the proposed discrete wavelet transforms (DWT) based VLC system. In the suggested scheme, the IDFT/DFT blocks utilized in the traditional system (Fig. 1) are substituted by the IDWT/DWT blocks which in turn eliminate the usage of the CP. To explain the working of IDWT/DWT blocks a brief introduction of wavelets is necessary.

A wavelet is referred to as a wave of small duration that has finite energy focused around a point in time and thus provides a means for the investigation of non-stationary, transient, and time-varying phenomena [33, 34]. It offers the characteristics that are similar to an oscillating wave and has the potential to permit concurrent analysis both in time and frequency-domain. Due to this fact, wavelets become a strong contender that can replace Fourier analysis. A wavelet is represented by a window function that splits the user information into completely different frequency bands and thereafter, analyses the selected band of interest [35].

The fundamentals of DWT started in 1976 when Crosier, Esteban, and Galand conceived a method of decomposing a discrete-time signal [36]. The DWT of the given discrete signals is computed by decomposing the signal into distinct frequency bands by succeeding high and low pass filter banks. These two filters are also known as the Quadrature Mirror Filter (QMF) pair and the process of decomposition is termed as sub-band coding
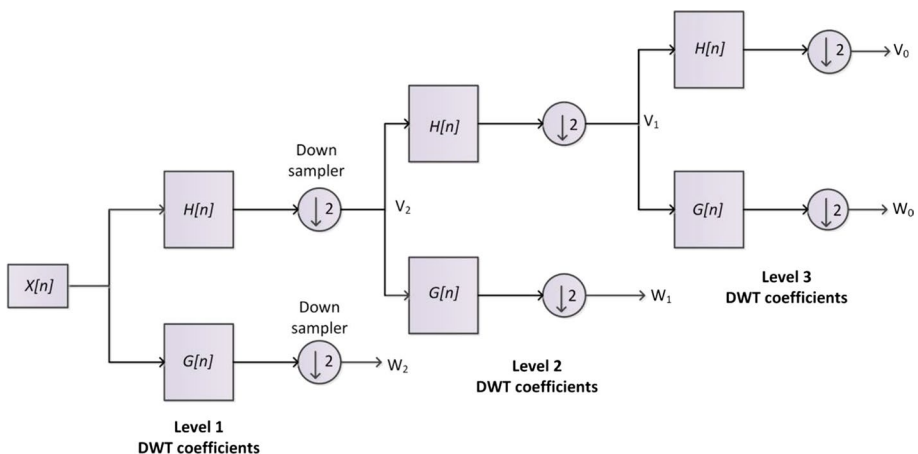

Fig. 2 Three level signal decomposition

[37]. On passing through low pass filter, high frequencies components are blocked and it contains only slowly changing information of the signal also termed as approximation coefficients (AC). While high pass filter stops low frequencies components and yields detailed coefficients (DC) that are rapidly changing components of the signal. Figure 2 shows the three-level decomposition of the input signal. However, the decomposition procedure can be elongated based upon at what level of precision and accuracy in the results are required.

An information signal $X[n]$ is input to filter banks that comprise high $G[n]$ and lowpass $H[n]$ filters respectively [37]. For analysis at the first level, $X[n]$ is split into a pair of equal high and low-frequency components. The higher frequency components due to less information can be discarded while lower frequency has a lot of information and thus it can be further processed. It is pertinent to discuss here that due to the removal of high-frequency components samples within the signal are reduced which results in the reduction of sampling rate and therefore, the time resolution becomes half while the spectral resolution is doubled [38].

At the next level, the output of $H[n]$ is sampled by factor 2 to satisfy the Nyquist criterion and again decomposed in high and low-frequency components. In the same manner, the decomposition process continues at the third level. Mathematically, the process of decomposition is given as [39, 40]:

$$W_{high}[k] = \sum_n D[n]G[2k - n] \tag{1}$$

$$V_{low}[k] = \sum_n D[n]H[2k - n] \tag{2}$$

The operation of inverse DWT is converse to DWT. In IDWT, the operation of downsampling is replaced by upsampling.

2.3 VLC Channel Model

In VLC systems, an air interface is used as a communication medium. Owing to the natural randomness in our surroundings, it is difficult to receive the exact message which was originally transmitted. Therefore, it is of great importance that the channel characteristics need to be identified to maximize the error performance of the VLC system. An indoor VLC channel model is categorizing into directed/LoS and non-directed/NLoS paths [41, 42]. The overall impulsive response of the VLC channel is computed by summing up the individual responses of both configurations. Mathematically, the cumulative VLC channel response is expressed as:

$$h(t) = H_{LoS}\delta(t - \tau_{LoS}) + H_{NLoS}\delta(t - \tau_{NLoS}) \tag{3}$$

where $H_{LoS}\delta(t - \tau_{LoS})$ is the impulsive response due to the LoS signal while $H_{NLoS}\delta(t - \tau_{NLoS})$ is the response due to the reflections. Also, the parameters τ_{LoS} and τ_{NLoS} represents the delay for the first incoming LoS and NLoS signal, moving from LED towards the photo-diode. The LoS path is realized as a point-to-point link in which a VLC transmitter can communicate with the receiver through narrow beams. This would mean that there exist no obstacles in the LoS link and for this reason, it is free from the reflections. In the LoS scenario, the signal attenuation is depending upon the path-loss that can
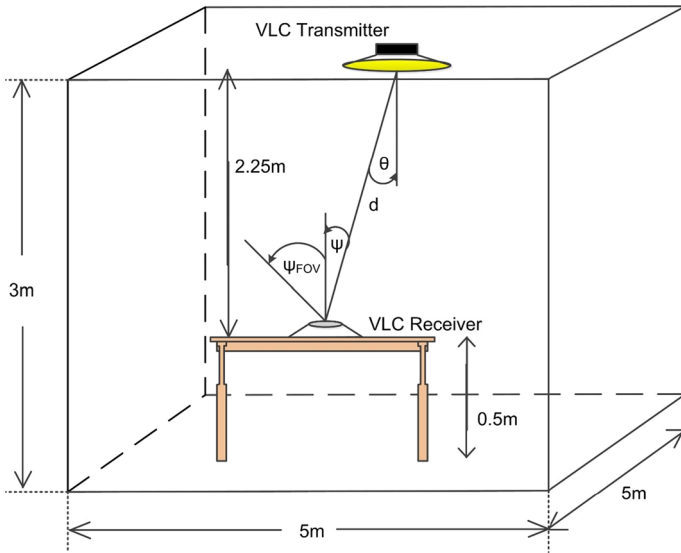
Fig. 3 VLC channel model

be evaluated by utilizing the knowledge of distance and beam divergence between transmitter and receiver. The LoS link is demonstrated in Fig. 3 in which an LED transmitter is considered as a monochromatic source having a Lambertian radiation pattern. Mathematically, the channel DC gain H_{LoS} for LoS link is given as [43, 44]:

$$H_{LoS} = \frac{(m_e + 1) * A_d}{2\pi d^2} * cos^{m_e}(\theta) * \cos(\Psi) * g(\Psi) * T(\Psi) \tag{4}$$

where A_d denotes the area of photo-diode, d shows the separation between the emitter and detector, Ψ and θ express the incidence and irradiance angle respectively, $g(\Psi)$ denotes the gain of a concentrator, $T(\Psi)$ illustrates optical filter gain. The aforesaid Eq. 4 is valid only when the incidence angle is less than Field of View (Ψ_{FOV}) i.e., $\Psi < \Psi_{FOV}$. The parameter m_e recognizes the Lambertian emission and it is expressed as [43]:

$$m_e = \frac{-\ln(2)}{\ln\left(\cos\left(\theta_{1/2}\right)\right)} \tag{5}$$

where $\theta_{1/2}$ shows the half-power angle of the LED. The current work only deals with the LoS link as it carries nearly 95% of the entire optical power. As we are dealing only with the LoS link, the Eq. 3 can be rewritten in the simplified form as:

$$h(t) = H_{LoS}\delta\left(t - \tau_{LoS}\right) \tag{6}$$

$$h(t) = \frac{(m_e + 1) * A_d}{2\pi d^2} * cos^{m_e}(\theta) * \cos(\Psi) * g(\Psi) * T(\Psi)\left(t - \tau_{LoS}\right) \tag{7}$$

3 Performance Evaluation for MC-CDMA Systems

This section is aimed to provide the complete analytical derivations of BER for MC-CDMA systems discussed in Sect. 2. We first analytically evaluate the performance of the traditional MC-CDMA system in the presence of the LoS channel and then correlate it for the proposed systems.

3.1 Analytical Derivation of BER for Traditional MC-CDMA System

In a typical MC-CDMA modem, the data is transmitted in N narrowband sub-carriers. Nonetheless, due to the Hermitian symmetry constraint, only $N/2$ sub-carriers are transmitting the data while other $N/2$ sub-carriers transmit complex conjugation of first $N/2$ sub-carriers. Hence, the transmitted MC-CDMA signal $S_m(t)$ can be articulated as:

$$S_m(t) = \sqrt{\frac{2P}{N}} \sum_{k=0}^{\frac{N}{2}} b_k[n]c_k[n]\cos\left(\omega_n t\right)P_T(t) \tag{8}$$

where N designates the number of sub-carriers (equals to the size of FFT transform), P signifies the power of the data bit, $b_k[n]$ denotes the uniformly distributed incoming data bit where $b_k \in (0, 1)$ with $E[b_k[n]] = 0$ and $E\left[|b_k[n]|^2\right] = 1$, $c_k[n]$ epitomizes the spreading sequence, ω_n is the angular frequency of the nth sub-carrier and, $P_T(t)$ represents the rectangular pulse which is non-zero in the interval [0, T].

For IM/DD based optical wireless link, the received signal $r(t)$ before the channel equalization can be summarized as:

$$r(t) = RS_m(t) \otimes h(t) + \eta(t) \tag{9}$$

where $S_m(t)$ is the transmitted MC-CDMA signal, $h(t)$ is the impulse response of the VLC channel, R represents the responsitivity of the photo-diode, the symbol $\otimes$ signifies the convolution operator and $\eta(t)$ is the shot noise modeled as Gaussian noise with zero mean and variance [43].

$$\sigma_{shot}^2 = 2qRP_r B + N_0 I_2 B \tag{10}$$

where q is the electron charge, P_r designates the received optical power, B denotes the equivalent noise bandwidth, N_0 signifies the noise density, and I_2 epitomizes the noise bandwidth factor. By replacing the $S_m(t)$ in Eq. 9 with its actual value (Eq. 8), the received signal can be given as:

$$r(t) = R\sqrt{\frac{2P}{N}} \sum_{k=0}^{\frac{N}{2}} b_k[n]c_k[n]\cos\left(\omega_n t\right)P_T(t-\tau) \otimes h(t) + \eta(t) \tag{11}$$

where τ indicates the time delay facing by the optical signal in moving from the transmitter LED to the receiver photo-diode. In our case, we assume $\tau = 0$ because of perfect synchronization between the VLC transmitter and receiver. To derive the analytical BER for the MC-CDMA system, a random variable must be obligatory that is not accessible for the LoS link because of all the parameters given in Eq. 7 are known and fixed. So, in this

scenario, the only random variable available for BER derivations is $\eta(t)$. For zero-forcing equalizer, the channel equalization coefficients $c(t)$ must satisfy,

$$h(t) \otimes c(t) = \delta \tag{12}$$

where δ symbolizes the Dirac delta function. The received signal after the equalization is specified as:

$$r_e(t) = c(t) \otimes r(t) = RS_m(t)c(t) \otimes h(t) + c(t) \otimes \eta(t) \tag{13}$$

$$r_e(t) = RS_m(t) + \eta(t) \tag{14}$$

$$r_e(t) = R\sqrt{\frac{2P}{N}} \sum_{k=0}^{\frac{N}{2}} b_k[n]c_k[n] \cos\left(\omega_n t\right) P_T(t) + \eta(t) \tag{15}$$

Using some results given in [12], the decision variable used to estimate the k th bit is given as,

$$V_0 = \frac{1}{T} \int_0^T r_e(t) \sum_{i=1}^{\frac{N}{2}} c[i] \cos\left(\omega_i t\right) dt \tag{16}$$

$$V_0 = \frac{1}{T} \int_0^T \left(R\sqrt{\frac{2P}{N}} \sum_{k=1}^{\frac{N}{2}} b_k[n]c_k[n]\cos\left(\omega_n t\right) P_T(t) + \eta(t) \right) \sum_{i=1}^{\frac{N}{2}} c[i] \cos\left(\omega_i t\right) dt \tag{17}$$

$$V_0 = \sum_{k=1}^{\frac{N}{2}} \sum_{i=1}^{\frac{N}{2}} \frac{R}{T}\sqrt{\frac{2P}{N}} b_k[n]c_k[n]c[i] \int_0^T \cos\left(\omega_n t\right) \cos\left(\omega_i t\right) + \sum_{i=1}^{\frac{N}{2}} \int_0^T \eta(t)\cos\left(\omega_i t\right) dt \tag{18}$$

It is imperative to mention here that multiplying the Gaussian variable with any signal does not change the statistics of the Gaussian noise and thus it remains the same. Therefore, the simplified form of the decision variable given in [12] can be written as,

$$V_0 = D + I + \eta \tag{19}$$

where I is the multiple access interference which is not considered in this work as the system is designed just for the single user, η is the corresponding noise term and D indicates the desired signal which is computed when the variable $k = i$,

$$D = R\sqrt{\frac{2P}{N}} \sum_{k=1}^{\frac{N}{2}} (c[k])^2 b_k[n] = R\sqrt{\frac{2P}{N}} b_k[n] \tag{20}$$

The energy of the desired bit, E_b, can be calculated as,

$$E_b = E\{|D|^2\} = \left(R\sqrt{\frac{2P}{N}} \right)^2 = \frac{2PR^2}{N} \tag{21}$$

By employing the Eqs. 10 and 21 the signal-to-noise ratio (SNR) is defined as,

$$SNR = \frac{\frac{2PR^2}{N}}{\sigma^2_{shot}} \tag{22}$$

For $M-$ ary rectangular QAM modulation with an even number of bits per symbol, the analytical BER can be obtained by the renowned relation [45],

$$BER_{M-QAM} = \frac{2\left(\sqrt{M}-1\right)}{\sqrt{M}log_2(M)} Q\left(\sqrt{\frac{3SNR}{2(M-1)}}\right) \tag{23}$$

In the above relation, $Q(x)$ is given by,

$$Q(x) = \frac{1}{2\pi} \int\limits_{x}^{\infty} e^{\frac{-y^2}{2}} dy \tag{24}$$

3.2 Analytical Derivation of BER for Proposed ESIM Based FT-MC-CDMA System

The existing subsection acquaints with the analytical BER for ESIM based FT-MC-CDMA system. For generalization, a single sub-carrier pair is transmitted and received through an LoS-VLC channel. As fading is not considered in this work, therefore, the data is corrupted
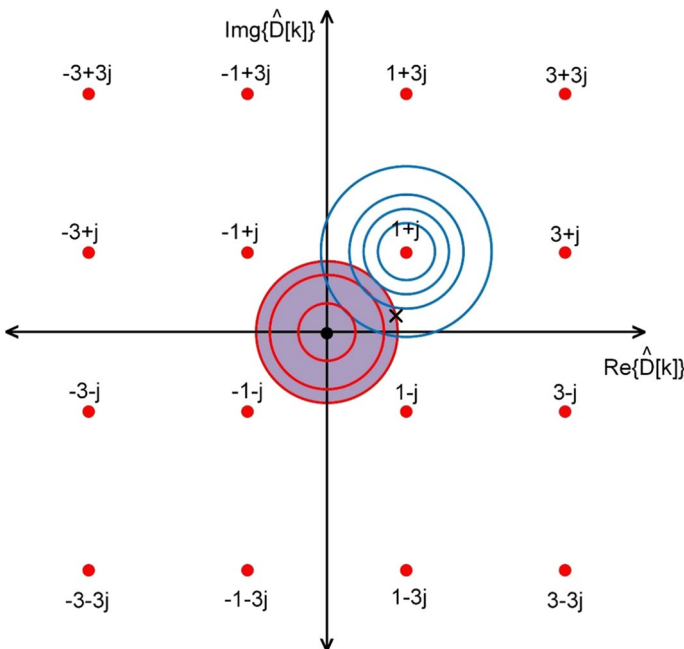

Fig. 4 Contour lines of distribution for received sub-carrier pair

by the AWGN channel as discussed in the previous subsection. The BER equations derived in this section are similar for all other sub-carrier pairs. Now consider that a QAM symbol '1 + j' is transmitted with inactive sub-carrier of the pair. The contour lines of distribution of received sub-carriers are displayed in Fig. 4 in which an active sub-carrier is indicated by a mark '×' and mathematically, it is denoted as $\hat{D}[k]$ that takes a value of $p + jq$. The decision for an inactive sub-carrier is considered as correct only when all possible values lie inside the shaded circle. Therefore, the integration of the shaded region of the circle provides the probability for accurately identifying active and inactive sub-carrier within a pair. The results of integration can be understood from [46] and are expressed as:

$$P_r\{b_k = 1|\hat{D}[k] = p + jq\} = \int\limits_{-\sqrt{|p+jq|^2}}^{\sqrt{|p+jq|^2}} \int\limits_{-\sqrt{|p+jq|^2-b^2}}^{\sqrt{|p+jq|^2-b^2}} \frac{1}{\pi\sigma_n^2} e^{-(a^2+b^2)\big/\sigma_n^2} da \cdot db \qquad (25)$$

By converting the Cartesian coordinates to polar coordinates, the aforesaid equation (Eq. 25) can be simplified as [47]:

$$P_r\{b_k = 1|\hat{D}[k] = p + jq\} = \int\limits_{0}^{2\pi} \int\limits_{0}^{\sqrt{|p+jq|^2}} \frac{1}{\pi\sigma_n^2} e^{-\frac{r^2}{\sigma_n^2}} r dr \cdot d\theta \qquad (26)$$

$$P_r\{b_k = 1|\hat{D}[k] = p + jq\} = 1 - e^{-\frac{|p+jq|^2}{\sigma_n^2}} \qquad (27)$$

For accurately identifying the active sub-carrier $b_k = 1$. It is important to discuss here that when AWGN is not added to the signal, then there is an equal probability that a sub-carrier is correctly identified from M constellation points. Therefore, the probability density of the received sub-carrier is the weighted sum of M distinct probability densities originating from Gaussian functions. The probability density of received sub-carrier is given as [47]:

$$\hat{D}[k] = \frac{1}{M} \sum_{i=1}^{M} \frac{1}{\pi\sigma_n^2} e^{-\frac{(p-Re(\mu_i))^2+(q-Img(\mu_i))^2}{\sigma_n^2}} \qquad (28)$$

where μ signifies the constellation point, i refers to the number of constellation points and it varies from 1 to M, $Re(\mu_i)$ denotes the real part of the constellation point and, $Img(\mu_i)$ gives an imaginary part.

By using Eqs. 27 and 28, the probability for correctly identifying active and passive sub-carrier is formulated as [47]:

$$P_r\{b_k = 1\} = \int\limits_{-\infty}^{\infty} \int\limits_{-\infty}^{\infty} P_r\{b_k = 1|\hat{D}[k]\} * P_r\{\hat{D}[k] = p + jq\} dx \cdot dy \qquad (29)$$

$$P_r\{b_k = 1\} = \int\limits_{-\infty}^{\infty} \int\limits_{-\infty}^{\infty} 1 - e^{-\frac{|p+jq|^2}{\sigma_n^2}} * \frac{1}{M} \sum_{i=1}^{M} \frac{1}{\pi\sigma_n^2} e^{-\frac{(p-Re(\mu_i))^2+(q-Img(\mu_i))^2}{\sigma_n^2}} \qquad (30)$$

The simplification of Eq. 30 yields:

$$P_r\{b_k = 1\} = 1 - \frac{1}{2M} \sum_{i=1}^{M} e^{-\frac{|\mu_i|^2}{2\sigma_n^2}} \tag{31}$$

While the probability of incorrect identification of active and inactive sub-carrier is given as [47]:

$$P_r\{b_k = 0\} = 1 - P_r\{b_k = 1\} \tag{32}$$

$$P_r\{b_k = 0\} = 1 - \left[1 - \frac{1}{2M} \sum_{i=1}^{M} e^{-\frac{|\mu_i|^2}{2\sigma_n^2}}\right] \tag{33}$$

$$P_r\{b_k = 0\} = \frac{1}{2M} \sum_{i=1}^{M} e^{-\frac{|\mu_i|^2}{2\sigma_n^2}} \tag{34}$$

The overall error performance of the ESIM-OFDM system is assessed through probability density equations which are already computed in Eqs. 31 and 34. If the state of the sub-carrier is not correctly identified then the corresponding OOK bit that encodes the sub-carrier state also detected as wrong. The BER which is contributed by this erroneous OOK bit is formulated as [47]:

$$BER_{OOK} = P_r\{b_k = 0\} * \frac{1}{log_2(M) + 1} \tag{35}$$

$$BER_{OOK} = \frac{1}{2M\left(log_2(M) + 1\right)} \sum_{i=1}^{M} e^{-\frac{|\mu_i|^2}{2\sigma_n^2}} \tag{36}$$

The BER analysis of QAM symbol is similar to the analysis already done in [47] which is mathematically expressed as:

$$BER_{QAM} = P_r\{b_k = 0\} * \frac{1}{log_2(M) + 1} + P_r\{b_k = 1\} * BER_{M-QAM} \frac{log_2(M)}{log_2(M + 1)} \tag{37}$$

Next, by employing the Eqs. 23, 31, and 34, The aforesaid Eq. 37 can be written in the simplified form as,

$$BER_{QAM} = \frac{1}{2M\left(log_2(M) + 1\right)} \sum_{i=1}^{M} e^{-\frac{|\mu_i|^2}{2\sigma_n^2}} + \frac{2\left(\sqrt{M} - 1\right)}{\sqrt{M}\left(log_2(M) + 1\right)} Q\left(\sqrt{\frac{3SNR}{2(M - 1)}}\right)$$
$$- \frac{\left(\sqrt{M} - 1\right)}{M\sqrt{M}\left(log_2(M) + 1\right)} Q\left(\sqrt{\frac{3SNR}{2(M - 1)}}\right) \sum_{i=1}^{M} e^{-\frac{|\mu_i|^2}{2\sigma_n^2}} \tag{38}$$

The final expression that yields the complete BER of ESIM-OFDM is formulated as [47]:

$$BER_{ESIM-OFDM} = BER_{OOK} + BER_{QAM} \tag{39}$$

3.3 Analytical Derivation of BER for Proposed ESIM Based WT-MC-CDMA System

From Sect. 2.2 it is apparent that in wavelet analysis the input signal is linearly convolved with the QMF filter bank. Nonetheless, the linear convolution yields an output signal with excessive length. To circumvent this, circular convolution is more preferable for wavelet analysis. Consider a QMF filter with length L in which the last $\frac{L}{2}$ components resulted because of linear convolution are added to first $\frac{L}{2}$ components. To ensure the perfect reconstruction of the signal, $\frac{L}{2}$ the left circular shift is essential to carry out for the input of each DWT procedure [48]. As in the proposed WT based MC-CDMA system, the complex sinusoids of FFT are replaced with the QMF filter pair, therefore, the noise acting on each sub-carrier must be different. To derive the exact BER equation, we first determine the noise variance. Also, to make the model simple we only demonstrated the derivations using the QMF filter for AC components. The DC components are derived by a similar process.

The circular shift can be represented by a specific permutation and for this reason, the DWT operation is defined as $\zeta(j, S) \cong \left(j + \frac{L}{2}\right) \mod S$. By taking the circular shift of the noise term in Eq. 13, each element in the input signal can be signified as [48],

$$\eta_m(t) = c_{\zeta\left(m, \frac{N}{2}\right)} \otimes \eta(t)$$

$$\eta_m(t) = \sum_n c_{\zeta\left(m, \frac{N}{2}\right)-n} \eta(t) \tag{40}$$

$$\eta_m(t) = \sum_n c_{m+\zeta\left(-n, \frac{N}{2}\right)} \eta(t)$$

For the analysis of the AC part, a low pass filter $G[n]$ is used and the circular convolution of two series a and b with period N is defined as $a_n \otimes b_n = \sum_m a_m b_{n-m}^N$. The downsampling operation is indicated by the operator $\downarrow$. The DWT for the first level is given as [48],

$$al1_m = (\eta_m(t) \otimes G_m) \downarrow 2$$

$$al1_m = \sum_n \left(\sum_k c_{\zeta\left(n, \frac{N}{2}\right)-k} \cdot \eta(t)\right) G_{2m-n} \tag{41}$$

$$al1_m = \sum_k \eta(t) \sum_n c_{\zeta\left(n, \frac{N}{2}\right)-k} G_{2m-n}$$

As the noise term is Gaussian distribution with zero mean, therefore, the mean value of $al1_m$ is also zero. However, the variance can be found as,

$$Var\{al1_m\} = E\{al1_m^2\} - \left(E\{al1_m\}\right)^2 = E\{al1_m^2\}$$

$$Var\{al1_m\} = \sum_k \eta^2(t)\left(\sum_n c_{\zeta\left(n,\frac{N}{2}\right)-k}G_{2m-n}\right)^2$$

$$Var\{al1_m\} = \delta^2 \sum_k \left(\sum_n c_{\zeta\left(n,\frac{N}{2}\right)-k}G_{-n}\right)^2$$

$$Var\{al1_m\} = \delta^2 \sum_k \left(\sum_n c_{\zeta+k\left(-n,\frac{N}{2}\right)}G_{-n}\right)^2 \qquad (42)$$

$$Var\{al1_m\} = \delta^2 \sum_k \left(\sum_n c_{\zeta\left(k,\frac{N}{2}\right)-n}G_n\right)^2$$

$$Var\{al1_m\} = \delta^2 \sum_k \left(c_{\zeta\left(k,\frac{N}{2}\right)} \otimes G_k\right)^2$$

Similarly, the variance of multi-level DWT can be computed. Using the tree structure of DWT and some useful results obtained through [48] the noise variance for $N = 64$ and 3-level DWT can be computed as,

$$N_0 = V_W(m, N=64, L=3) = \begin{cases} Var\left(ag1_m\right) & 0 \le m < 32 \\ Var\left(ag2_m\right) & 32 \le m < 48 \\ Var\left(ag3_m\right) & 48 \le m < 56 \\ Var\left(ah3_m\right) & 56 \le m < 64 \end{cases} \qquad (43)$$

The SNR equation is derived in Eq. 22 remains the same, however, the only change is the change in noise variance. Further, the exact BER equation for ESIM based WT-MC-CDMA is also similar to the Eq. 38.

4 Simulation Results and Discussions

The current section is distributed into three sub-sections wherein the initial section elaborates on the simulation setup. This section also gives the channel parameters essential for the characterization of the LoS link. The second sub-section offers a statistical analysis of visible light characteristics from LED lightings. The characteristics of visible light within a room are the distribution of transmitter illuminance (lm), received power distribution (dBm), coverage area (m), and variations of received power concerning LED's semi angle at half power (degrees) and receivers FOV. While the third section conveys the simulation results and discussions on traditional OFDM based MC-CDMA, ESIM based DFT-MC-CDMA, and ESIM based proposed DWT-MC-CDMA based on numerous performance metrics. Although, it is shown in [29, 32] that ESIM performs better than traditional OFDM. However, the author believes that this is the first work on ESIM based MC-CDMA. So, to assess its performance, simulations of the traditional MC-CDMA system are also conducted.

Table 1 Simulation parameters for conventional and proposed MC-CDMA systems

Simulation parameters	OFDM based FT-MC-CDMA	ESIM based FT-MC-CDMA	ESIM based WT-MC-CDMA
Number of MC-CDMA symbols	10^4	10^4	10^4
Spreading code	7-bit OOC	7-bit OOC	7-bit OOC
Modulation	16-ary and 64-ary QAM	16-ary and 64-ary QAM	16-ary and 64-ary QAM
Sub-carriers	64	64	64
CP length	1/4th	1/4th	Not required
MC-CDMA symbol length	80 samples	80 samples	64 samples
Wavelet type	Haar, Daubechies (db2), Symlet (sym2), Coiflet (coif2), Biorthogonal (bior1.1, bior3.3), Reverse Biorthogonal (rbio1.1, rbio3.3), Discrete Meyer (dmey)		
VLC channel	LoS		
Room Size	5 m×5 m×3 m		
LED placement	(2.5, 2.5, 2.75)		
The separation between Tx and Rx	2.15 m		
Receiver above the floor	0.5 m		
Number of LEDs	10×10 (100)		
Transmitted power	300 W		
Optical lens gain	10		
Noise type	AWGN		
SNR (dB)	0–20		
Equalizer	Zero forcing		

4.1 Simulation Setup

For performance assessments, the computer-based programs for traditional and proposed systems are formulated in MATLAB tool with the LoS VLC channel. The parameters required for the simulations of all systems are recorded in Table 1 whereas the simulation setup is exhibited in Fig. 3. For the LoS link, a vacant room with measurements of 5 m×5 m×3 m is considered. A VLC transmitter is affixed on the ceiling at an elevation of 2.75 m above the floor emitting light in the downward direction whereas a user terminal equipped with photo-diode is positioned on the desk at the height of 0.5 m from the floor. Thus, the total communication distance of the directed path is 2.25 m.

To make the channel simulation realistic, OSW4XME3C1S cool white star-shaped off-the-shelf LEDs are selected for the transmitter while silicon pin photo-diodes S6775 are used to gather the optical signals. In a transmitter, the LEDs are arranged in an array of 10×10. Each LED provides the luminous flux of 200 lm which is sufficient to illumine the room [49]. OSW4XME3C1S LED is easily accessible in a market with a broader viewing angle of 120° and emits an optical power of 3 W. The S6775 photo-diode is manufactured by the Hamamatsu in a clear plastic package with an effective area of 26.4 mm^2 [50]. The spectral response range and peak sensitivity wavelength of S6775 are 320 nm to 1100 nm

Table 2 Specifications of LED and photo-diode

	Specifications	Values
OSW4XME3C1S LED	Semi angle	70°
	Emitted power by each LED	3 W
	Luminous flux	200 lm
	Forward voltage	3.3 V
	Operating current	800 mA
	Temperature sensitivity	-40 °C to 85 °C
S6775 Photo-diode	Field of view	70°
	Active area	26.4 mm^2
	Spectral response	320 nm to 1100 nm
	Photosensitivity	0.7 A/W
	Reverse voltage	35 V
	Operating temperature	-25 °C to 85 °C

and 960 nm respectively. While the photosensitivity of the photo-diode is 0.7A/W. The other specifications of the used LEDs and photo-diodes are also listed in Table 2.

The transmitter of each system communicates 10^4 MC-CDMA symbols. Under the simulation parameters mentioned in Table 1, the OFDM and ESIM based MC-CDMA transmitter generates binary random bits that are moved within one symbol. On these data bits, the procedure of MC-CDMA discussed in Sect. 2 is executed. The modulated waveform is then conveyed through the free-space LoS VLC channel. In the receiver design, a sub-optimal time-domain zero forcing equalizer is employed that nullifies the adverse effects of the channel. For all simulations, it is also considered that the emitter and receiver are well synchronized with each other. The BER results are acquired using Monte-Carlo simulations.

4.2 Statistical Analysis of Visible Light Characteristics

This section presents the results and discussions about visible light characteristics. For the given setup, computer-based simulations for the illuminance distribution within a room are carried out in MATLAB and a 3D based numerical result is plotted in Fig. 5. From this result, it is perceptible that the VLC transmitter offers sufficient illuminance at the boundaries of the room, thereby, making the communication possible. The maximum illuminance of about 86.52 lm is realized in the middle of the room. However, on heading towards the boundaries, illuminance is decreasing having a value of 13.39 lm.

Figure 6 exhibits the 3D plot of the received power distribution with and without a lens. In both cases, the power received is concentrated in the center of the room where the transmitter is installed. Nevertheless, power reduces when moving away from the center. It can be grasped from the result that with 100 LEDs the maximum power received without a lens at the center of the room is 0.1884 dBm and it is around -9.66 dBm at the boundaries of the room. Figure 6 also displays the received power graph when a lens is considered at the receiver. For this situation, the power received at the center of the room is 10.19 dBm while at the boundaries it is 0.34 dBm. From both results, it is evident that to realize efficient communication the receiver should be fitted out with a lens that focusses the optical signals on the photo-diodes.
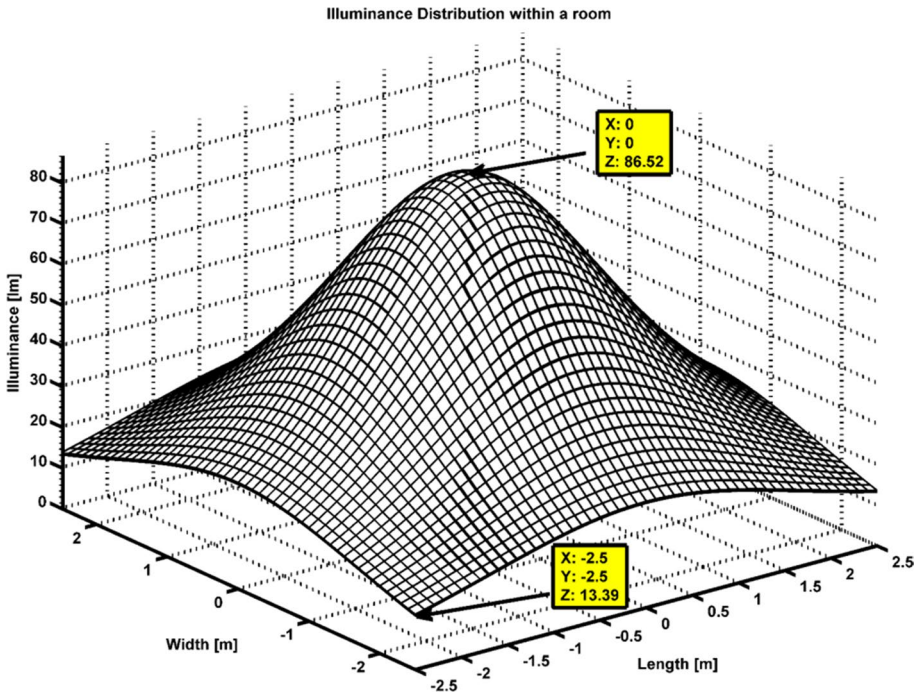
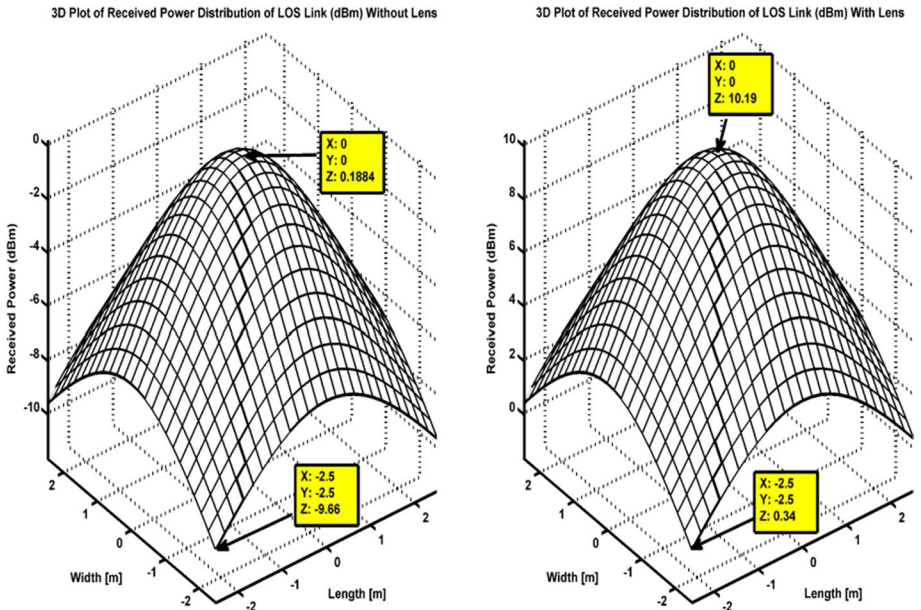**Fig. 5** Distribution of illuminance within a room

Fig. 6 Received power distribution within a room

The subsequent result Fig. 7, illustrates the coverage area of the room with reverence to the received power. It is worth mentioning from the contour lines-based result that the proposed setup of the LED transmitter provides the complete coverage of optical power to the users. Although, the optical power at the boundaries is lesser than the power at the center, however, it is still enough to achieve successful communication.

Figure 8 exhibits the result of the received power with and without optical lens at various semi angles at half power. For simulations, the FOV of the receiver and channel distance is fixed at 70° and 2.25 m respectively. Further, the VLC transmitter power is also fixed at 300 W, however, the semi angle of the LED varies from 5° to 70° with the range difference of 5°. The result shows that for both cases (with and without optical lens) the maximum power is received at a semi angle of 5°. By increasing the semi angle, the received power in the LoS link will become lesser. This is because by deviating the semi angle from 0° the optical radiation within the room becomes more diffusive and thus some of the optical transmitter power is captivated by the non-reflective objects.

The next result Fig. 9 demonstrates the received power with and without optical lens at numerous FOV angles. As it is observed in the previous result (Fig. 8) that the maximum power is received at lower semi angles so for simulations the LED semi angle is
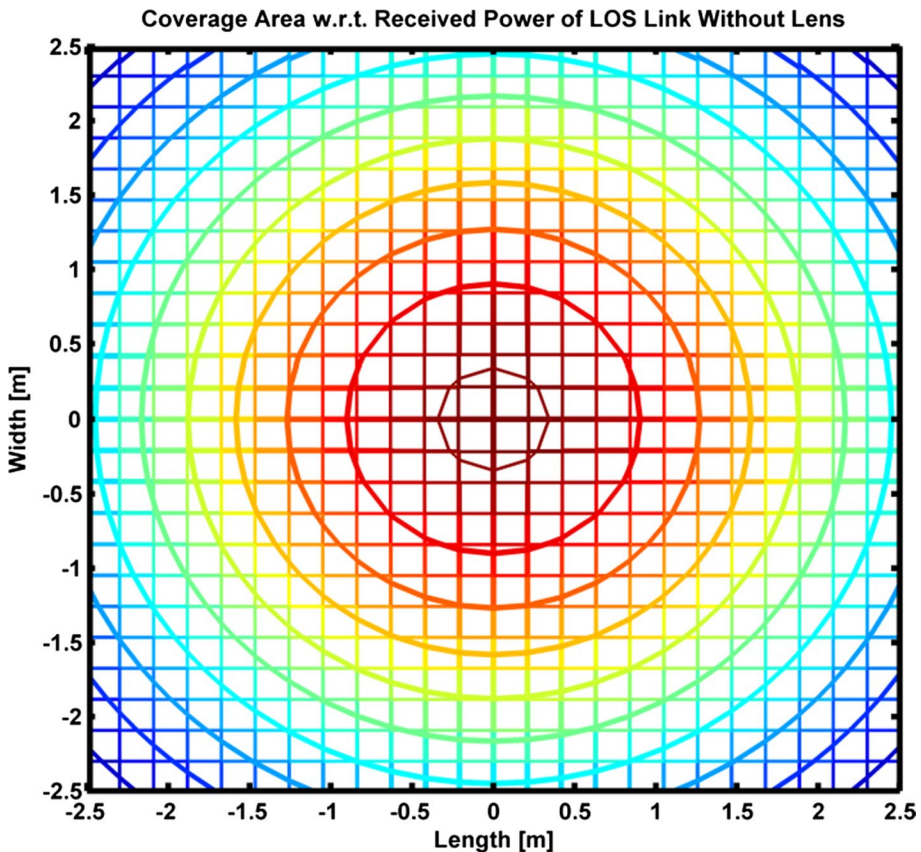

Fig. 7 Coverage area distribution concerning received power

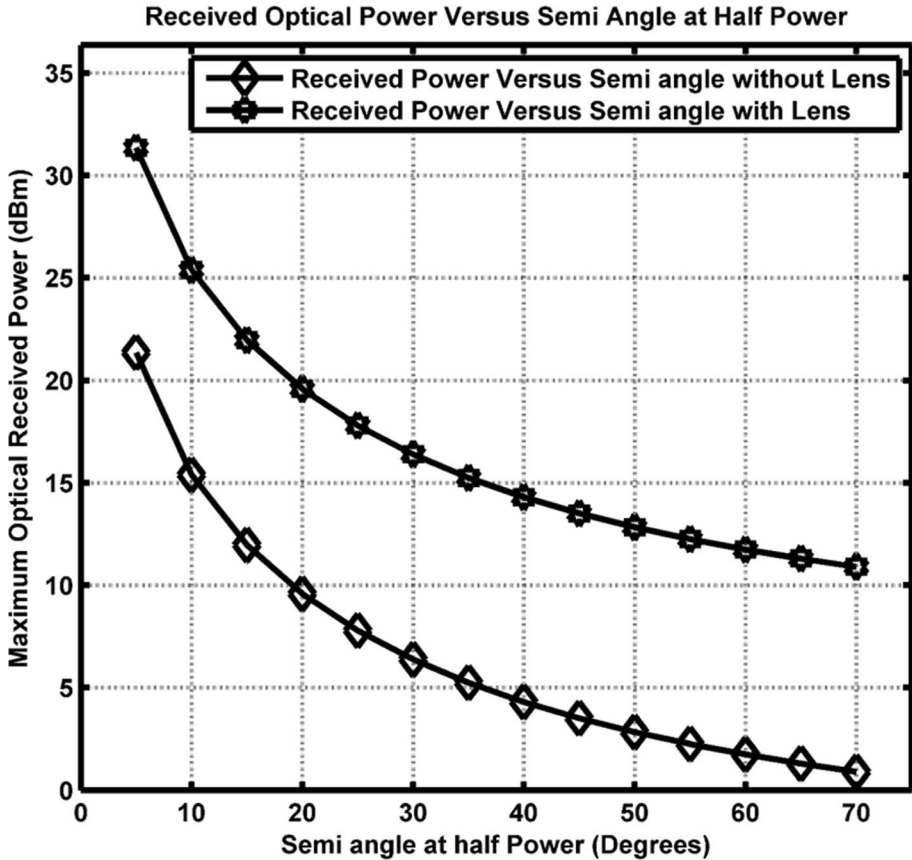**Received Optical Power Versus Semi Angle at Half Power**

Fig. 8 Effects on received power by varying LED semi angle

fixed at 10°. Moreover, the distance and transmitted power are also fixed as discussed previously. It has been depicted from the simulation result that the characteristics of the FOV on the photo-diode are slowly affecting the received power.

4.3 Results for Performance Comparison

The proposed ESIM based MC-CDMA system is assessed based on BER and PAPR metrics. Depending on the results shown in Figs. 8 and 9 the LED semi angle and FOV are fixed at 10° and 30° respectively. A series of simulations are run on MATLAB where the transmitter and receiver separation are 2.25 m. For DWT analysis, 'Haar' and other orthogonal wavelet families with different vanishing moments are selected. Figure 10 displays the plot for one MC-CDMA symbol generated by ESIM based MC-CDMA techniques. The QAM modulation order is fixed to 16 and the sub-carrier length is 64. Further, the x-axis of the graph shows the time axis while the y-axis epitomizes the voltage level. It can be evident from the time-domain spectra that after adding the DC bias there still exits some negative peaks which are clipped at zero. Also, the analysis of the spectra confirms that for ESIM based FT-MC-CDMA, the peak voltage level is 1.788 V while for
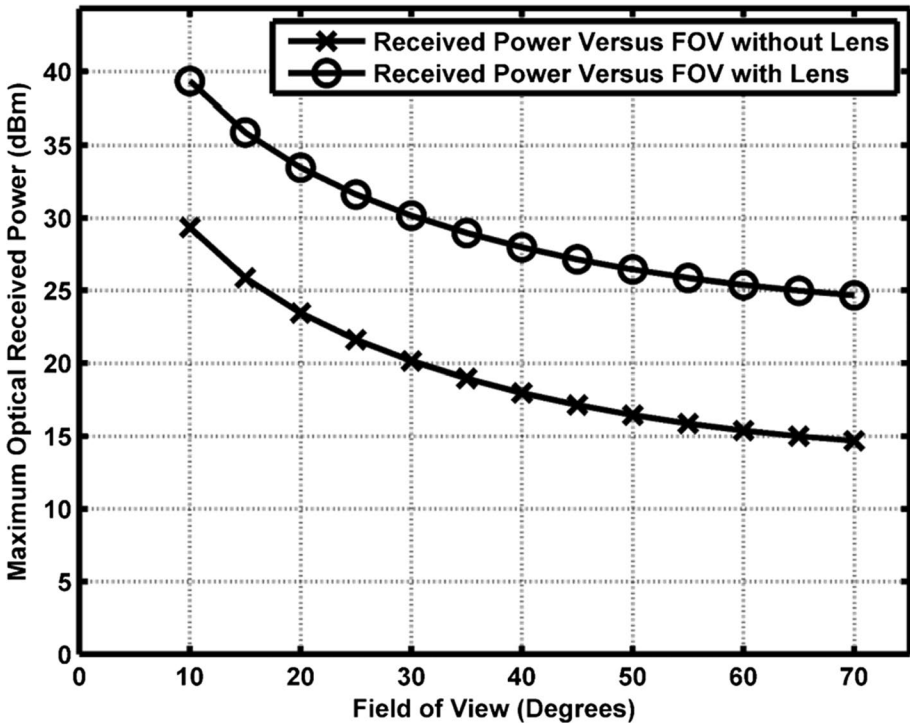
Fig. 9 Effects on received power by varying FOV of the receiver

WT-MC-CDMA, the voltage is 1.117 V. Hence, the PAPR of FT-MC-CDMA is high as compare to WT-MC-CDMA.

The simulations are also conducted to verify the BER expressions (Eqs. 23, 39, and 43) that are derived in Sect. 3. For the simulations, the applied QAM sizes are 16-QAM and 64-QAM while the sub-carrier size is 64. Moreover, the wavelet analysis is conducted by considering the Haar wavelet with level 2. The analytical and Monte-Carlo based simulated BER outcomes of the simulations are exhibited in Fig. 11. By comparing the analytical and simulated results, it can be noticed that analytical BER curves fit well with the simulated curves.

Next, the simulated results are also inspected for the targeted BER of 10^{-4} and it should be perceived that for the same QAM modulation order i.e., 16-QAM, the ESIM based FT-MC-CDMA needs less energy and performs approximately 2 dB superior to its counterpart OFDM based FT-MC-CDMA system. The error performance of the ESIM based FT-MC-CDMA system is further enhanced by replacing the Fourier transform with the wavelet transforms. The results illustrate that the proposed ESIM based WT-MC-CDMA system outperforms the ESIM based FT-MC-CDMA system and accomplishes a coding gain of approximately 4.4 dB. However, in comparison with OFDM based FT-MC-CDMA, this coding gain is 6.5 dB. It is noteworthy here that this performance improvement is due to the inherent orthogonal ability of wavelet transform which, unfortunately, could not be portrayed by Fourier transform. The similar improvements in the BER results could also be seen for high orders of M i.e., 64-QAM.
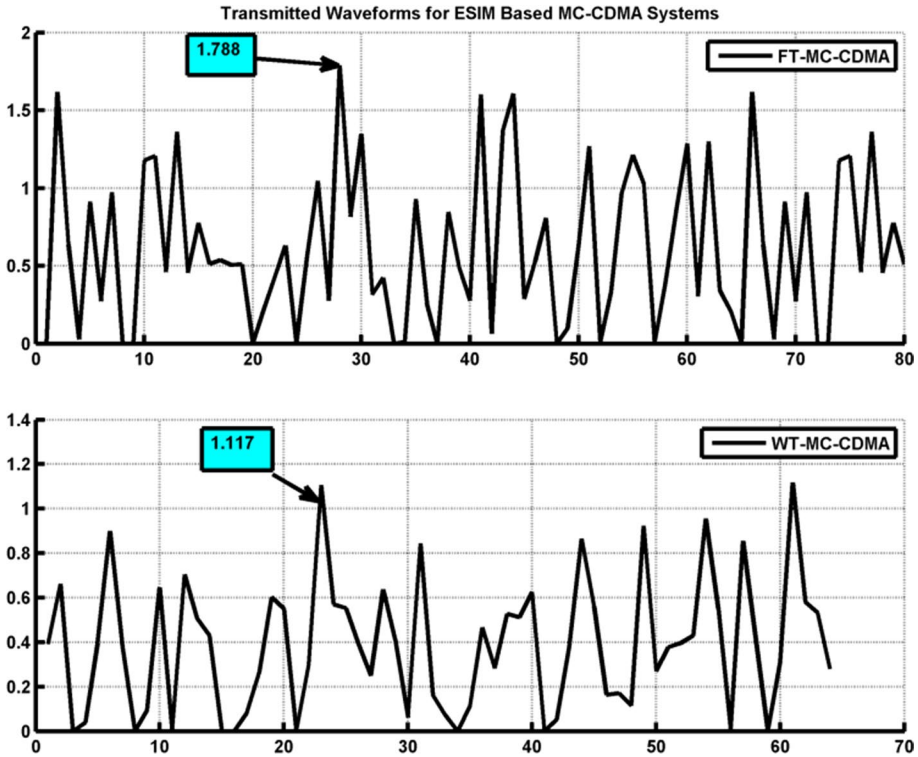
Fig. 10 Transmitted waveforms for a single sub-carrier of ESIM based MC-CDMA systems

Keeping in view the superior performance of wavelet-based multi-carrier systems, ESIM based WT-MC-CDMA is also simulated with the different wavelet families listed in Table 1. The effectiveness of the ESIM based WT-MC-CDMA system with different wavelet families are exhibited in Fig. 12. A very interesting fact can be deduced from the results as for all listed wavelet families the performance of the system is exactly similar except for the biorthogonal and reverse orthogonal wavelets with vanishing moments 3.3. Though the error performance of bior3.3 and rbio3.3 are similar to each other while this performance is about 2 dB poor than other wavelet families.

The MATLAB codes for the calculation of PAPR of the discussed systems are also developed and simulated. As observed from Fig. 10 that the high peaks in multi-carrier systems occur randomly, therefore, complementary cumulative distribution function (CCDF) is one of the best options to describe the PAPR. It is defined as the probability that illustrates the obtained PAPR exceeds a specific value $PAPR_0$. Mathematically [51],

$$CCDF = P_r(PAPR > PAPR_0) \tag{44}$$

Figure 13 shows the graphs for CCDF versus PAPR of traditional and suggested systems. These graphs are attained by considering the QAM modulation order of 16 and sub-carrier size $M = 1024$. The graphs illustrate that the PAPR of proposed ESIM based FT-MC-CDMA is reduced than traditional OFDM based MC-CDMA. On the other
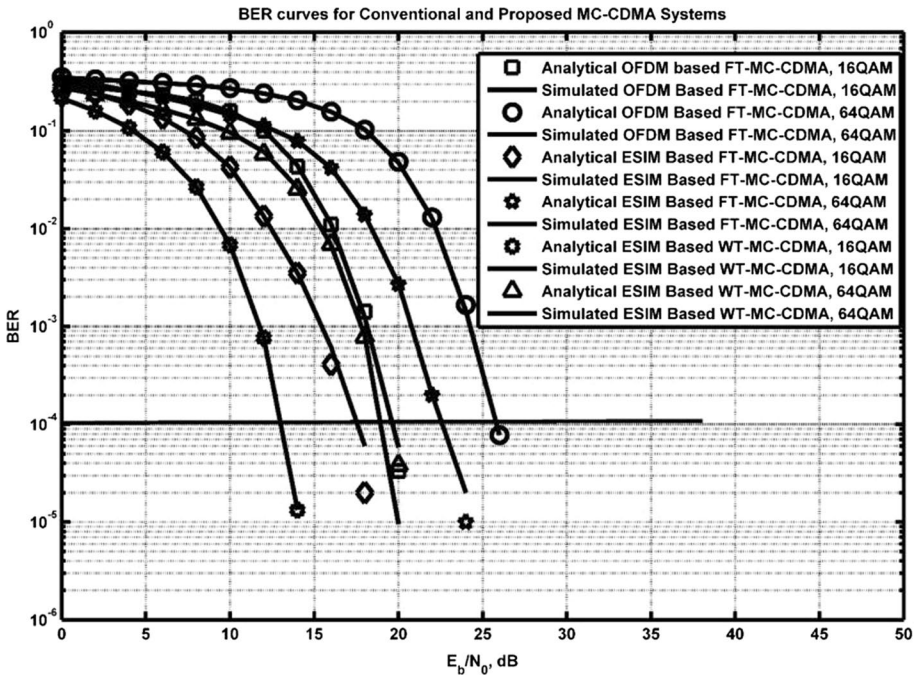
Fig. 11 Analytical and theoretical comparisons between proposed ESIM based MC-CDMA and conventional OFDM based MC-CDMA systems

hand, the PAPR performance of the system is enriched by using wavelets. The PAPR of ESIM based DWT-MC-CDMA is 4.5 dB reduced than traditional MC-CDMA and achieves CCDF of 10^{-4} at 11 dB.

5 Conclusions

Owing to the inherent merits, VLC is deemed as a success key in the implementation of attocells used within the upcoming 5G standards. In VLC systems, the placement of LEDs and photo-diodes within a room (attocell) plays a pivotal role in the reception of power at the boundaries of the room. Moreover, the use of an optical lens in the designing of the
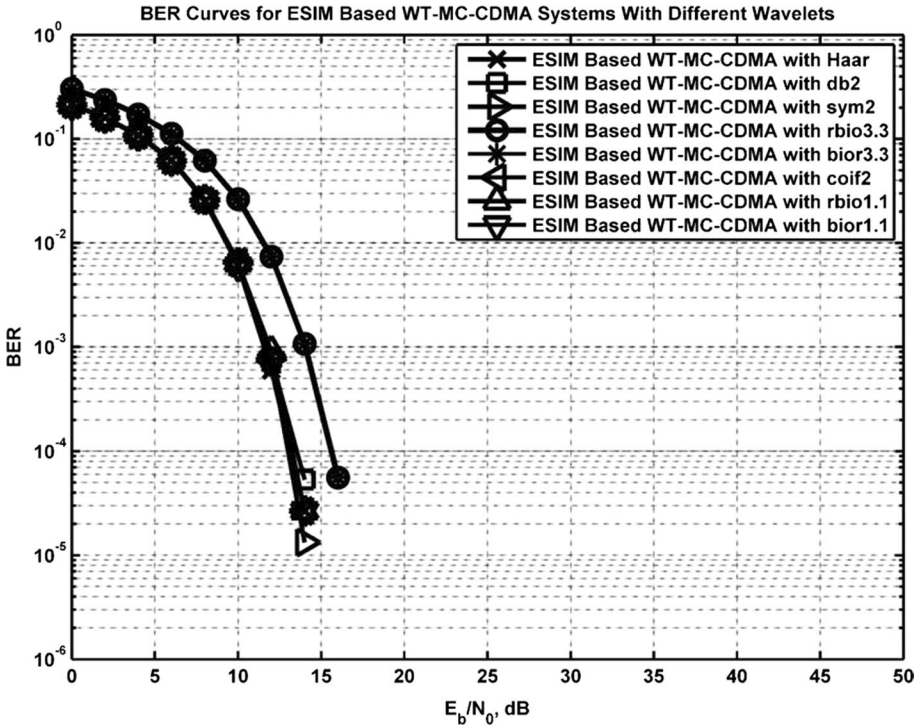
Fig. 12 Effectiveness of ESIM based WT-MC-CDMA with different wavelet families

VLC receiver also helps in focusing the optical power at photo-diodes. With the given settings, the simulation results display that the received power at the boundaries of the room is 0.34 dBm and coverage is satisfactory.

With the help of DWT and an improved version of OFDM (ESIM), a novel VLC system is designed and simulated. The work also includes the BER derivations for the ESIM based WT-MC-CDMA system which are validated by a comparison between simulations and analytical computations. The simulations are accomplished via MATLAB tool and it is examined through the comparison results that analytical BER curves fit well to the simulated curves. Moreover, the effectiveness of the suggested system is estimated concerning PAPR and BER. The simulated outcomes for proposed and conventional systems are also compared. The results also confirm that the ESIM based WT-MC-CDMA system outperforms other MC-CDMA systems. It is also concluded that inherent time–frequency localization properties of DWT reduce noise from the system, which ultimately eliminates the need for cyclic prefix and conserve the energy and bandwidth. Moreover, the CCDF graphs also demonstrate that PAPR of ESIM based MC-CDMA system reduces than OFDM based MC-CDMA system. Hence, the proposal of both ESIM and DWT schemes in the MC-CDMA structure is acceptable and the improvement in results demonstrates that the wavelet transform has a bright future in the field of VLC. Due to the noise suppression capability of wavelets, they are best
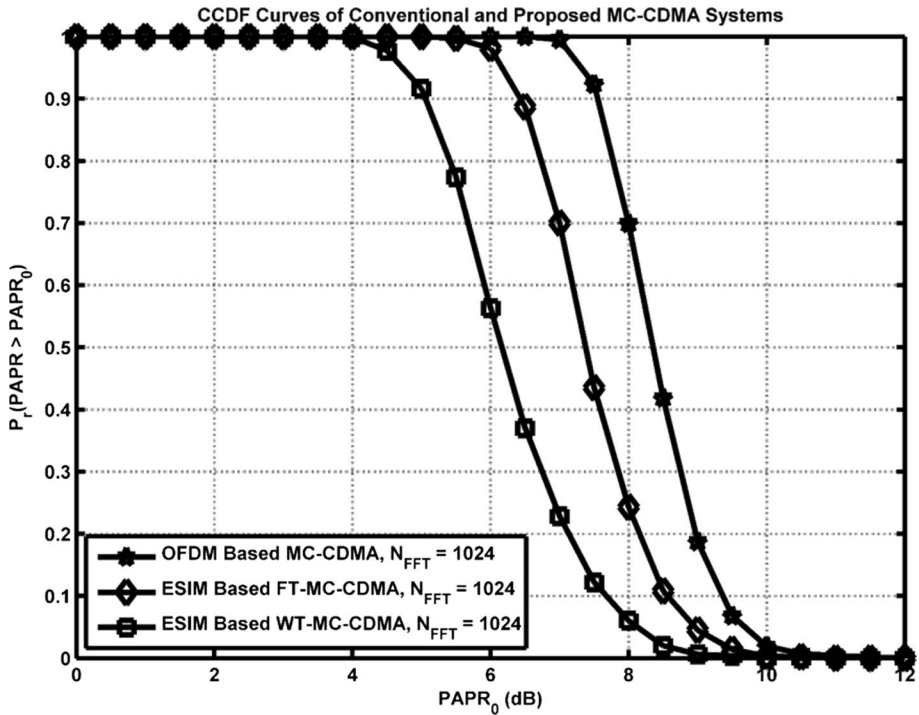
Fig. 13 PAPR versus CCDF plots for DFT and DWT based ESIM MC-CDMA systems

suited in VLC based indoor localization system. The future work includes a low cost and efficient hardware implementation that strengthen the proposed technique.

Compliance with Ethical Standards

Conflict of interest The author(s) declare(s) that there is no conflict of interest regarding the publication of this paper.

References

1. Mumtaz, S., Bo, A., Al-Dulaimi, A., & Tsang, K. F. (2018). Guest editorial 5G and beyond mobile technologies and applications for industrial IoT (IIoT). *IEEE Transactions on Industrial Informatics, 14*(6), 2588–2591.
2. Sharma, B., Saini, R. K., Singh, A., & Singh, K. K. (2020). Deep reinforcement learning for wireless network. *Machine Learning and Cognitive Computing for Mobile Communications and Wireless Networks., 17,* 51–71.
3. Yan, P., Choudhury, S., Al-Turjman, F., & Al-Oqily, I. (2020). An energy-efficient topology control algorithm for optimizing the lifetime of wireless ad-hoc IoT networks in 5G and B5G. *Computer Communications, 159,* 83–96.
4. Tabrizi, H. O., & Al-Turjman, F. (2020). AI for dynamic packet size optimization of batteryless IoT nodes: A case study for wireless body area sensor networks. *Neural Computing and Applications, 7,* 1–2.

5. Saadi, M., & Wuttisittikulkij, L. (2019). Visible light communication-the journey so far. *Journal of Optical Communications, 40*(4), 447–453.

6. O'Brien, D., Parry, G., & Stavrinou, P. (2007). Optical hotspots speed up the wireless communication. *Nature Photonics, 1*(5), 245.

7. Randel, S., Sierra, A., Mumtaz, S., Tulino, A., Ryf, R., Winzer, P. J., Schmidt, C., & Essiambre, R. J. (2012). Adaptive MIMO signal processing for mode-division multiplexing. In *OFC/NFOEC*. IEEE (pp. 1–3).

8. Ma, J., Li, K., Tan, L., Yu, S., & Cao, Y. (2016). Exact error rate analysis of free-space optical communications with spatial diversity over gamma-gamma atmospheric turbulence. *Journal of Modern Optics, 63*(3), 252–260.

9. Niaz, M. T., Imdad, F., Kim, S., & Kim, H. S. (2016). Deployment methods of visible light communication lights for energy-efficient buildings. *Optical Engineering, 55*(10), 106113.

10. Wang, C. X., Haider, F., Gao, X., You, X. H., Yang, Y., Yuan, D., et al. (2014). Cellular architecture and key technologies for 5G wireless communication networks. *IEEE Communications Magazine, 52*(2), 122–130.

11. Qiu, Y., Chen, S., Chen, H. H., & Meng, W. (2017). Visible light communications based on CDMA technology. *IEEE Wireless Communications, 25*(2), 178–185.

12. Shoreh, M. H., Fallahpour, A., & Salehi, J. A. (2015). Design concepts and performance analysis of multicarrier CDMA for indoor visible light communications. *Journal of Optical Communications and Networking, 7*(6), 554–562.

13. McCormick, A. C., & Al-Susa, E. (2002). Multicarrier CDMA for future generation mobile communication. *Electronics and Communication Engineering Journal, 14*(2), 52–60.

14. Liao, H., Zhou, Z., Zhao, X., Zhang, L., Mumtaz, S., Jolfaei, A., et al. (2019). Learning-based context-aware resource allocation for edge-computing-empowered industrial IoT. *IEEE Internet of Things Journal, 7*(5), 4260–4277.

15. Priyanjali, K. S., & Ramanjaneyulu, B. S. (2017). Performance of MC-CDMA system with various orthogonal spreading codes in a multipath Rayleigh fading channel. In: *International conference on smart technologies and management for computing, communication, controls, energy, and materials (ICSTM), IEEE* (pp. 309–312).

16. Soundararajan, R., Kumar, S. R., Gayathri, N., & Al-Turjman, F. (2020). Skyline query optimization for preferable product selection and recommendation system. *Wireless Personal Communications., 18,* 1–8.

17. Kondo, S., & Milstein, B. (1996). Performance of multicarrier DS CDMA systems. *IEEE Transactions on Communications, 44*(2), 238–246.

18. Taher, M., Singh, M., Ismail, M., Samad, S. A., & Islam, M. T. (2013). Sliding the SLM-technique to reduce the non-linear distortion in OFDM systems. *Elektronika ir Elektrotechnika, 19*(5), 103–111.

19. Bolcskei, H., Duhamel, P., & Hleiss, R. (2001). A subspace-based approach to blind channel identification in pulse shaping OFDM/OQAM systems. *IEEE Transactions on Signal Processing, 49*(7), 1594–1598.

20. Yu, J. L., & Chen, C. H. (2008). A low-complexity block linear smoothing channel estimation for SIMO-OFDM systems without cyclic prefix. *IEICE Transactions on Communications, 91*(4), 1076–1083.

21. Meng, Y., Wang, J., Zhu, J., & Wang, H. (2008). Blind multiuser detection using the subspace-based linearly constrained LSCMA. *Signal Processing, 88*(9), 2246–2253.

22. Wu, X., Yin, Q., Zhang, H., & Deng, K. (2002). Time-domain multiuser detection for MC-CDMA systems without cyclic prefix. In *International conference on communications, ICC 2002, IEEE* (vol. 2, pp. 921–925).

23. Daly, D., Heneghan, C., & Fagan, A. D. (2004). Minimum mean-squared error impulse response shortening for discrete multitone transceivers. *IEEE Transactions on Signal Processing, 52*(1), 301–306.

24. Jones, A. E., Wilkinson, T. A., & Barton, S. (1994). Block coding scheme for reduction of peak to mean envelope power ratio of multicarrier transmission schemes. *Electronics Letters, 30*(25), 2098–2099.

25. Saeedi, H., Sharif, M., & Marvasti, F. (2002). Clipping noise cancellation in OFDM systems using oversampled signal reconstruction. *IEEE Communications Letters, 6*(2), 73–75.

26. Muller, S. H., & Huber, J. B. (1997). OFDM with reduced peak-to-average power ratio by optimum combination of partial transmit sequences. *Electronics Letters, 33*(5), 368–369.

27. Bauml, R. W., Fischer, R. F., & Huber, J. B. (1996). Reducing the peak-to-average power ratio of multicarrier modulation by selected mapping. *Electronics Letters, 32*(22), 2056–2057.

28. Zhang, H., Zhang, J., & Qiu, K. (2014). Performance comparison of wavelet packet transform-based and conventional coherent optical OFDM transmission system. *Optik, 125*(11), 2647–2651.

29. Ahsan, M., & Asif, H. M. (2017). ESIM-OFDM-based transceiver design of a visible light communication system. *International Journal of Communication Systems, 30*(8), e3175.
30. Dang, J., Wu, L., & Zhang, Z. (2017). OFDM systems for optical communication with intensity modulation and direct detection. *Optical Fiber and Wireless Communications, 85,* 111–117.
31. Dissanayake, S. D., & Armstrong, J. (2013). Comparison of ACO-OFDM, DCO-OFDM and ADO-OFDM in IM/DD systems. *Journal of Lightwave Technology, 31*(7), 1063–1072.
32. Khalid, A., & Asif, H. M. (2018). OCDMA and OSTBC based VLC transceiver design using NI cDAQ. *Photonic Network Communications, 35*(1), 97–108.
33. Burrus, C. S., Gopinath, R. A., Guo, H., Odegard, J. E., & Selesnick, I. W. (1998). *Introduction to wavelets and wavelet transforms: A primer* (p. 1). New Jersey: Prentice Hall.
34. Lakshmanan, M. K., & Nikookar, H. (2006). A review of wavelets for digital wireless communication. *Wireless Personal Communications, 37*(3–4), 387–420.
35. Kaiser, G. (2010). *A friendly guide to wavelets*. Berlin: Springer Science & Business Media.
36. Polikar, R. (1998). *Multi-resolution analysis: The discrete wavelet transform, the wavelet tutorial part IV*. Rowan University, College of Engineering Web Servers (p. 10).
37. Baig, S., Asif, H. M., Umer, T., Mumtaz, S., Shafiq, M., & Choi, J. G. (2018). High data rate discrete wavelet transform-based PLC-VLC design for 5G communication systems. *IEEE Access, 6,* 52490–52499.
38. Li, A., Shieh, W., & Tucker, R. S. (2010). Wavelet packet transform-based OFDM for optical communications. *Journal of Lightwave Technology., 28*(24), 3519–3528.
39. Guillen, D., Idarraga-Ospina, G., & Cortes, C. (2016). A new adaptive mother wavelet for electromagnetic transient analysis. *Journal of Electrical Engineering, 67*(1), 48–55.
40. Khan, A., Arif, A., Nawaz, T., & Baig, S. (2017). Walsh Hadamard transform based transceiver design for SC-FDMA with discrete wavelet transform. *China Communications, 14*(5), 193–206.
41. Chvojka, P., Zvanovec, S., Haigh, P. A., & Ghassemlooy, Z. (2015). Channel characteristics of visible light communications within a dynamic indoor environment. *Journal of Lightwave Technology, 33*(9), 1719–1725.
42. Pesek, P., Zvanovec, S., Chvojka, P., Bhatnagar, M. R., Ghassemlooy, Z., & Saxena, P. (2018). Mobile user connectivity in relay-assisted visible light communications. *Sensors, 18*(4), 1125.
43. Komine, T., & Nakagawa, M. (2004). Fundamental analysis for a visible-light communication system using LED lights. *IEEE Transactions on Consumer Electronics, 50*(1), 100–107.
44. Lee, K., Park, H., & Barry, J. R. (2011). Indoor channel characteristics for visible light communications. *IEEE Communications Letters, 15*(2), 217–219.
45. Vitthaladevuni, P. K., Alouini, M.-S., & Kieffer, J. C. (2005). Exact BER computation for cross QAM constellations. *IEEE Transactions of Wireless Communication, 4*(6), 3039–3050.
46. Alouini, M. S., & Goldsmith, A. J. (1999). A unified approach for calculating error rates of linearly modulated signals over generalized fading channels. *IEEE Transactions on Communications, 47*(9), 1324–1334.
47. Tsonev, D., Sinanovic, S., & Haas, H. (2011). Enhanced subcarrier index modulation (SIM) OFDM. In *GLOBECOM workshops (GC Wkshps), IEEE* (pp. 728–732).
48. He, Q., Schmitz, C., & Schmeink, A. (2013). BER of Fourier transform and discrete wavelet transform based OFDM, ISWCS 2013. In *The tenth international symposium on wireless communication systems, Ilmenau, Germany* (pp. 1–5).
49. OptoSupply, OSW4XME3C1S LED. (2012). https://www.alldatasheet.net/datasheet-pdf/pdf/352547/OPTOSUPPLY/OSW4XME3C1S.html.
50. Hamamatsu Photon, Si PIN Photodiode—S6775. (2014). https://www.hamamatsu.com/resources/pdf/ssd/s2506-02-etc-kpin1048e.pdf.
51. Musabe, R., Lionel, M. B., Ushindi, V. M., Atupenda, M., Ntaganda, J., & Bajpai, G. (2019). PAPR reduction in LTE network using both peak windowing and clipping techniques. *Journal of Electrical Systems and Information Technology, 6*(1), 3.

Arslan Khalid received the Bachelor's and Master's degrees in electrical engineering from the COMSATS University Islamabad, Lahore campus, Pakistan, in 2012 and 2016, respectively. Mr. Khalid is currently pursuing his Ph.D. Degree from the School of Information, Computer, and Communications Technology (ICT), Sirindhorn International Institute of Technology, Thailand. He has more than five years of the optical wireless industry and academic experience and has published several papers in well-reputed Journals and InternationalConferences. In 2017, Mr. Khalid had joined the Department of Electrical Engineering, The University of Lahore, Pakistan as a Lecturer. From 2012 to 2017, he was with the Department of Electrical and Computer Engineering, COMSATS Institute of Information Technology, Pakistan. His research interests include communication theory, computer networks, wireless communication systems, visible light communication, Multicarriermodulation techniques such as OFDM and its variants, Wavelets and Wavelet transforms, Wavelet Transform based multi-carrier modulation techniques, Code Division MultipleAccess (CDMA) technology, Software Defined Radio (SDR), MIMO Systems such as Repetition Coding, Space-Time Block Coding (STBC), Spatial Multiplexing, Channel Modeling, Rank Codes, and their Applications, and Internet of Things (IoT).

Faizan Rashid was born in Lahore, Pakistan, He received his Bachelor's and Master's Degree in Electrical Engineering from The University of Lahore, Pakistan in 2011 and 2017 respectively. He is currently working as a Lecturer in the same university in the Electrical Engineering department. His research interest includes communication systems, visible light communications, software-defined radios, Multilevel Inverters, Distribution systems, Renewable energy resources, Circuit designing, and Machine design. He has also worked on MIMO systems and the internet of things. Currently, he is doing work on the integration of renewable energy resources such as Wind and Solar.

Umair Tahir has received his Bachelor's and Master's degrees in Electrical Engineering with distinction from The University of Lahore, Lahore, Pakistan in 2016 and 2019 respectively. He is currently serving as a Lecturer in the Department of Electrical Engineering at the University of Lahore, Lahore, Pakistan. He has publications in well reputed International Journals and IEEE International conferences. His research interests include power switching converters, applications of power electronics in modern power systems, communication systems, visible light communications, channel modeling, multi-carrier communications, and Internet of Things (IoT)

Hafiz M. Asif received the B.S. degree in electrical engineering from UET, Lahore, Pakistan, in 2002, the M.S. degree in computer engineering from the King Fahad University of Petroleum and Minerals (KFUPM), in 2007, and the Ph.D. degree in communication systems from Lancaster University, U.K., in 2012. He is currently with the Department of Electrical and Computer Engineering, Sultan Qaboos University, Oman. He has also worked in the Department of Electrical Engineering, Taif University (TU), Saudi Arabia. His research interests include visible light communication, space-time block codes, rank codes, wireless communication systems, and computer networks.

Dr. Fadi Al-Turjman received his Ph.D. in computer science from Queen's University, Kingston, Ontario, Canada, in 2011. He is a full professor and a research center director at Near East University, Nicosia, Cyprus. Prof. Al Turjman is a leading authority in the areas of smart/intelligent, wireless, and mobile networks' architectures, protocols, deployments, and performance evaluation. His publication history spans over 300 publications in journals, conferences, patents, books, and book chapters, in addition to numerous keynotes and plenary talks at flagship venues. He has authored and edited more than 30 books about cognition, security, and wireless sensor networks' deployments in smart environments, published by Taylor and Francis, Elsevier, and Springer. He has received several recognitions and best papers' awards at top international conferences. He also received the prestigious Best *Research Paper Award* from Elsevier Computer Communications Journal for the period 2015-2018, in addition to the *Top Researcher Award* for 2018 at Antalya Bilim University, Turkey. Prof. Al-Turjman has led several international symposia and workshops in flagship communication society conferences. Currently, he serves as an associate editor and the lead guest/associate editor for several well-reputed journals, including the *IEEE Communications Surveys and Tutorials* (IF 23.9) and the Elsevier Sustainable Cities and Society (IF 5.7).